JPE 13-4-2

http://dx.doi.org/10.6113/JPE.2013.13.4.516

Adaptive On-line State-of-available-power Prediction of Lithium-ion Batteries

Christian Fleischer[†,***], Wladislaw Waag[*,***], Ziou Bai[*], and Dirk Uwe Sauer[*,**,***]

[†*]Electrochemical Energy Conversion and Storage Systems Group, Institute of Power Electronics and Electrical Drives (ISEA), RWTH Aachen University, Germany

[**]Institute of Power Generation and Storage Systems (PGS), E.ON ERC, RWTH Aachen University, Germany

[***]Jülich Aachen Research Alliance, JARA-Energy, Germany

Abstract

This paper presents a new overall system for state-of-available-power (SoAP) prediction for a lithium-ion battery pack. The essential part of this method is based on an adaptive network architecture which utilizes both fuzzy model (FIS) and artificial neural network (ANN) into the framework of adaptive neuro-fuzzy inference system (ANFIS). While battery aging proceeds, the system is capable of delivering accurate power prediction not only for room temperature, but also at lower temperatures at which power prediction is most challenging. Due to design property of ANN, the network parameters are adapted on-line to the current battery states (state-of-charge (SoC), state-of-health (SoH), temperature). SoC is required as an input parameter to SoAP module and high accuracy is crucial for a reliable on-line adaptation. Therefore, a reasonable way to determine the battery state variables is proposed applying a combination of several partly different algorithms. Among other SoC boundary estimation methods, robust extended Kalman filter (REKF) for recalibration of amp hour counters was implemented. ANFIS then achieves the SoAP estimation by means of time forward voltage prognosis (TFVP) before a power pulse occurs. The trade-off between computational cost of batch-learning and accuracy during on-line adaptation was optimized resulting in a real-time system with TFVP absolute error less than 1%. The verification was performed on a software-in-the-loop test bench setup using a 53 Ah lithium-ion cell.

Key words: Adaptive neuro-fuzzy inference system, Battery monitoring; On-line estimation algorithm, Power prediction

I. INTRODUCTION

Among all battery technologies, lithium-ion batteries are considered by most of the car manufacturers to meet the HEV/EV requirements in the best way, because of their high energy and power density. Nevertheless, safety aspects still play an important role since lithium-ion batteries are subject to power limitations due to physical operation restrictions of the battery cells. Information about the state-of-charge (SoC), the state-of-health (SoH) and available power of the battery are important in order to operate electrical or hybrid vehicles at better cost effectiveness, more flexibility, optimal energy efficiency and with maximum of safety and comfort for the passengers. In order to ensure this lithium-ion battery packs must be equipped with a monitoring and safety device, the battery management system (BMS) running on a controller with integrated measuring electronics. The essential part of the BMS, however, are its corresponding algorithms for the status determination. Mobility, comfort and precision are central expectations that people have in HEV/EV application, inevitably leading the battery pack to deliver not only significant amount of energy to the loads, but also provide required power in every driving situation. To achieve high system voltages, many individual cells are connected in series. Due to the fact that individual cells in a battery differ in manufacturing and diverse progressive ageing, the overall available power of the battery pack is limited by individual maximum/minimum cell voltage, SOC, temperature ranges and finally the maximum current rating, which is compared to the previous restrictions authorized by the manufacturer. The maximum available power, e.g. for the next 10 to 20 seconds,

Manuscript received Jan. 24, 2013; revised Mar. 17, 2013
Recommended for publication by Associate Editor Jin Hur.
[†]Corresponding Author: batteries@isea.rwth-aachen.de
Tel: +49 241-8097158, ISEA
[*]Electrochemical Energy Conversion and Storage Systems Group, Institute of Power Electronics and Electrical Drives (ISEA), RWTH Aachen University, Germany
[**]Institute of Power Generation and Storage Systems (PGS), E.ON ERC, RWTH Aachen University, Germany
[***]Jülich Aachen Research Alliance, JARA-Energy, Germany

is also an important input to the energy management system (EMS) which controls and optimizes the power flow between electric consumers and distributed power sources. In this work, the available power is defined as an additional state: state-of-available-power (SoAP). For instance, before an overtaking maneuver, power prediction helps to avoid dangerous situations such as sudden power drops which may lead to a critical dynamic condition. In order to prevent a sudden voltage drop in the HV-DC link, the maximum available discharging/charging power that can be used for acceleration/regenerative braking has to be estimated by the BMS. This work presents a novel on-line method for an accurate state-of-available-power prediction. Due to its self-learning design property this adaptive method also considers the current ageing state and predicts critical situations by means of TFVP to react instantly and anticipates future power needs to the EMS. The paper is organized as follows. Section II gives an overview about the state of the art techniques for power prediction. Further, their disadvantages are discussed leading to the motivation to respond with a new improved method. Section III gives an overview about the supporting algorithms for SOC state estimation, which is an important input parameter for TFVP. Section IV describes the different specifications of power prediction and the proposed SoAP method. At the end of the paper the software-in-the-loop test bench setup is explained, which is used for verification purposes.

II. State of the Art Prediction of Available Power

Conventional state of the art methods for SoAP prediction can be categorized into two groups: 1.) techniques which are based on battery characteristic maps and 2.) techniques using equivalent circuit models to describe the battery dynamics. For the first group, extensive cell tests are carried out in advance to generate a dependency between the available power of the battery in regard to the battery states (eg. SoC, temperature), cell's voltage and power pulse parameters [12],[17]. These are then stored in characteristic maps (CM) in a non-volatile memory of the electronic control unit (ECU). These tests are performed at different SOC levels, at different temperatures (e.g. −20 °C up to 60 °C) applying different power pulses to cover the entire power spectrum of the cells. Different testing standards define the procedure for these hybrid pulse power characterization tests (HPPC) [18]–[20]. During the operating lifetime of the battery its characteristics change due to ageing [21]–[25], and the stored CM for the new battery becomes invalid. During operation, the measured battery power is compared to the predicted battery power. The estimation error $\tilde{P} = \hat{P}_{\text{predicted}} - P_{\text{measured}}$ is used to adapt the current reference point of the CM in order to improve the power prediction for next time. The added value of this technique lies

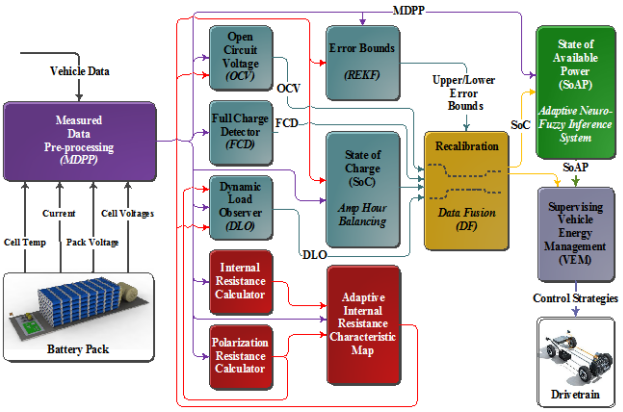

Fig. 1. Overall SoAP estimation with supporting algorithms.

in the simple implementation and handling. Here, no complex mathematical models have to be derived and therefore fast error analysis is possible. However, these advantages do not compensate for its weaknesses. Drawbacks here, CM may be based on synthetic profiles, which are not able to cover all real driving situations leading to static battery characteristics. Furthermore, the adaptation process may adapt infrequent occurrences of extreme load wrongly. This may be due to the fact that various polarization overvoltages which depend on the previous load history are not considered. Also, the adaptation procedure may lead to poor results in cases where the maximum available power has to be predicted, but can only be adapted when the maximum power is in fact applied to the battery. Their suggestions for adapting and optimizing the neighboring operating points are based on smoothing functions, which are not motivated on battery non-linear dynamics. The requirement of valuable non-volatile memory on the ECU is also a major drawback for these methods. Some ideas take further steps to make sure that no unnecessary memory usage occurs by approximating the CM with empirical functions [17], [26]. The second group of techniques is based on simplified dynamic battery models [27]–[35] which extrapolates future cell voltages with higher accuracy. These approaches differ in applied equivalent circuit models and methods for on-line parameter estimation. These parameter estimation use various versions of the recursive Kalman filter (KF) estimator, such as extended Kalman filter (EKF) considering non-linearities, sigma-point KF (SPKF) or joint and dual Kalman filter for state and parameter estimation. Some assumptions taken for KF are the measurement and model inaccuracies (noises) which are set to Gaussian probability density function (pdf), but may differ in real application. Moreover, the non-linearities (NL) are approximated using first-order (EKF) or second-order (SPKF) Taylor series expansion. Recent publications only apply NL to the SOC-OCV relation [37]–[39]. For a reliable power prediction using ECM also the current dependency has to be considered additionally. The general knowledge about the covariances and noises has to be known a priori. Wrong values may lead to poor convergence and slow adaptation. A further

possibility for integrating on-line adaptation of the ECM parameters is based on recursive least squares estimation (RLS) [40], [41] to fit the measured data to the ECM. To reduce the matrix operations a weighted recursive least squares (WRLS) estimation was proposed in [42], [43]. Both methods generally fit the data but without considering the current dependency which makes the ECM approach less reliable. Furthermore, the published work demonstrates the methods basically at room temperatures, where the current dependency of the resistance is less crucial to the battery dynamics. In practice these disadvantages of the described state of the art techniques cause defective fulfillment in accuracy at low temperatures and aged state which motived us to design a new technique. Our method provides a robust, adaptive SoAP prediction algorithm using a self-learning neuro-fuzzy inference system (ANFIS).

III. Robust Extended Kalman Filter Based SoC Correction

For the efficient utilization and safe operation, an accurate determination of the SoC is required, in particular for the introduced method in available power prediction. The presented battery monitoring system for SoAP estimation consists of a set of different algorithms illustrated in Fig. 1 and adapted from [1]. It combines the algorithms OCV method, full charge detector (FCD)/dynamic load observer (DLO), and as key function the Ah-balancing (AhB) method with REKF algorithm. At present, AhB is the most commonly used method for SoC estimation, since it is the most accurate technique for short-term calculations and defined as

$$SoC(t) = SoC(t_0) + \frac{1}{C_N}\int_{t_0}^{t_0+t} I_{bat}(d\tau)\cdot 100\% \qquad (1)$$

where $SoC(t_0)$ is the initial SoC, C_N the nominal capacity, and I_{bat} the charging/discharging current. The dynamic measurement of battery current and its time integration provides directly the information of SoC. The requirement for long-term accuracy depends on terminal measurement equipment. Errors due to noise, wide range in resolution or rounding leads to accumulated errors. AhB will gradually lose precision the longer the calculation lasts. Supporting algorithms are necessary and have been introduced in [1] and adapted by means of REKF for SoC recalibration. As mentioned earlier, KF works well when system model and noise statistics are known a priori. Wrong assumptions or changes during operation may lead to degradation of filter estimates. Besides analyzing the estimative hidden state SoC, we implement the REKF more robust to uncertainties in the system matrix, the measurement matrix, and noise covariances. It also provides dynamically the estimation error bounds (EB). The on-line procedure can be broadly depicted as follows: The OCV is measured at the battery terminal after a rest time t_0, the SoC value $\mathrm{SoC}(t_0)$ is then calculated according to the OCV procedure. $SoC(t_0)$ is updated between t_0 and t_1 by the REKF method to obtain $SoC(t_1)$. $SoC(t_2)$ is then determined using the AhB method using the initial SoC value of $SoC(t_1)$ and corrected again by REKF and supporting algorithms [1]. These steps are constantly executed until the battery reaches fully charged or discharged state.

A. Design of Robust Extended Kalman Filter

Kalman filter is an algorithm to estimate the inner states of a dynamic system recursively by means of a set of mathematical equations [6]. The optimal solution only holds when the model is accurate while the system- and measurement noise statistics are known. Unfortunately, these underlying assumptions are in fact seldom met. Commonly, the model is faced with non-deterministically describable disturbances (process noise (w_k) and measurement noise (v_k) [5]. Therefore, we design the filter in such a way, that it becomes more robust to uncertainties in covariances $w_k \sim (0, Q)$ and $v_k \sim (0, R)$. The filter is designed to guarantee the finite upper and lower bound on the estimation error for SoC recalibration. The considered uncertain system is represented by

$$x_{k+1} = Fx_k + w_k \qquad (2)$$
$$y_k = Hx_k + v_k \qquad (3)$$

where $x_k \in R^l$ and $y_k \in R^m$ represent the state and measurement vectors at time step k, F and H states the process and receptively the measurement matrix. These two noise processes must be mutually uncorrelated, zero mean, respectively, and they must have a white Gaussian probability distribution [2]. The structure of the filter can be classified into three types of equations, *initialization*, *prediction* and *estimation* as illustrated in Table I. REKF is designed in such a way, that the relation between process/measurement noise and estimation error is less than the tuning parameter ξ described in Table I. Therefore, ξ states the relative weight given to reduce the variation of the estimation error due to process or measurement noise fluctuations and chosen in such a way, that the performance and robustness is balanced [3],[14]. When $R = 0$ (no measurement noise), the error covariance P becomes [3]

$$P_{R=0} = (I - KH)FP_{R=0}F^{\mathrm{T}}(I - KH)^{\mathrm{T}} + (I - KH)Q(I - KH)^{\mathrm{T}} \qquad (4)$$

and setting $Q = 0$ (no process noise), equation for error covariance P becomes [3]

$$P_{Q=0} = (I - KH)FP_{Q=0}F^{\mathrm{T}}(I - KH)^{\mathrm{T}} + KRK^{\mathrm{T}} \qquad (5)$$

Therefore, the true estimation error covariance can be described as the sum of the assumed covariance and the difference. Then the change in the estimation error covariance is described as [3]

TABLE I
ROBUST EXTENDED KALMAN FILTER EQUATIONS [3], [14]

Type	*Equation*
Initialization ($k=0$)	$\hat{x}_0^+ = \mathrm{E}[x_0]$ $P_0^+ = \mathrm{E}[(x_0-\hat{x}_0)(x_0-\hat{x}_0)^2]$
Computation	$k = 1,2,3,\ldots$ Compute partial derivative matrices $F_{k-1} = \frac{\partial f_{k-1}}{\partial x}\Big\vert_{\hat{x}_{k-1}^+}$, $L_{k-1} = \frac{\partial f_{k-1}}{\partial w}\Big\vert_{\hat{x}_{k-1}^+}$
Prediction	$P_k^- = F_{k-1}P_{k-1}^+F_{k-1}^T + L_{k-1}Q_{k-1}L_{k-1}^T$ $\hat{x}_k^- = f_{k-1}(\hat{x}_{k-1}^+, u_{k-1}, 0)$ Compute partial derivative matrices $H_{k-1} = \frac{\partial h_k}{\partial x}\Big\vert_{\hat{x}_k^-}$, $M_k = \frac{\partial h_k}{\partial v}\Big\vert_{\hat{x}_k^-}$
Measurement update	$\hat{x}_k^+ = \hat{x}_k^- + G_k[y_k - h_k(\hat{x}_k^-, 0)]$ $P_k^+ = (I - G_kH_k)P_k^-$
Kalman gain Matrix	$G_k = P_k^-H_k^{\mathrm{T}}(H_kP_k^-H_k^T + M_kR_kM_k^{\mathrm{T}})^{-1}$
Tuning parameter ξ	$\rho\mathrm{Tr}(P) + (1-\rho)\mathrm{E}\{[\mathrm{Tr}(\Delta P)]^2\}$

$$\Delta P = \alpha P_{R=0} + \beta P_{Q=0} \tag{6}$$

where α and β are random variables with variances with $\sigma_{R=0}^2$, $\sigma_{Q=0}^2$. From these characteristics, the mean of the change of the tuning parameter becomes zero, while the variance is $\sigma_{R=0}^2\mathrm{Tr}^2(P_{R=0}) + \sigma_{Q=0}^2\mathrm{Tr}^2(P_{Q=0})$ [3]. Therefore, we are able to make the filter robust to uncertainties by minimizing the variance of the tuning parameter. To describe it differently, (1 - ρ) is the weighting factor to reduce the variance of P due to uncertainty changes in R and Q [3]. Decreasing ρ will enhance the robustness of the filter. To determine the SoC, a dynamic model of the battery in the form of state variable equation is required. Here, the generic model consists of a voltage source representing an open circuit voltage (OCV) which is a function of SoC. The RC element accommodates both the charge transfer, as well as the double layer capacitance where R_{CT} and R_{DL} are a function of SoC, T, and current flow direction. The ohmic resistance R_{i} occurs instantly and is also depended on SoC, T, and current flow direction.

At first, for the described battery model, the state signals and the output signals are identified. The state vector contains the states SoC and V_{RC} while the output vector only consists of the cell voltage. The state-space equation is summarized in equation (7)

$$\begin{bmatrix} SoC_{k+1} \\ V_{RC,k+1} \end{bmatrix} = \begin{bmatrix} 1 & 0 \\ 0 & 1 - \frac{T_{\mathrm{s}}}{R_{\mathrm{CT}}C_{\mathrm{DL}}} \end{bmatrix} \begin{bmatrix} SoC_k \\ V_{\mathrm{RC},k} \end{bmatrix} \begin{bmatrix} \frac{T_{\mathrm{s}}}{C_{\mathrm{N}}} \\ \frac{T_{\mathrm{s}}}{C_{\mathrm{DL}}} \end{bmatrix} I_k + \begin{bmatrix} w_{1,k} \\ w_{2,k} \end{bmatrix} \tag{7}$$

where the OCV and all overvoltages are described as

$$y_k = OCV(SOC_k) + V_{\mathrm{RC},k} + R_{\mathrm{i},k}I_k \tag{8}$$

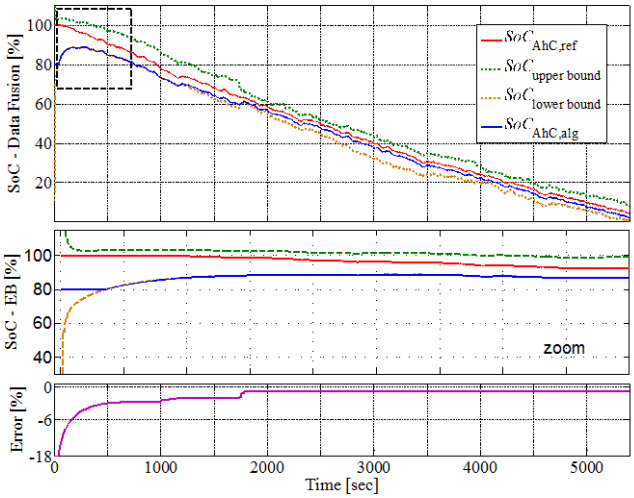

Fig. 2. Recalibration of *SoC* using REKF (wrong initial *SoC*=80 %).

The expression $\frac{dOCV}{dSoC}\Big\vert_k$ is calculated according to (9), whereas an infinite impulse response filter (IIR) is applied to avoid ripples.

$$\frac{dOCV}{dSoC}\Big\vert_k = \frac{OCV(SoC_k^-) - OCV(SoC_{k-1}^+)}{SoC_k^- - SoC_{k-1}^+} \tag{9}$$

Kalman filtering shall not provide an alternative SoC value to replace the AhB, instead error bounds (EB) are calculated to provide limits for the AhB SoC algorithm to allow recalibration. For that purpose, the state estimate error covariance matrix is used, which is a measure for the uncertainty of the state estimate [5]. The smaller the noise is, the more reliable are the state estimates. Consequently, the determination of the filter parameters such as Q and R plays an important role. The latter one can be determined very well, for instance by off-line measurement. The process noise covariance can hardly be measured but may be obtained by means of system identification using a further Kalman filter in off-line mode [16]. The corresponding error bounds ΔSoC_k at each time step are calculated in equation (10).

$$\Delta SoC_k = \sqrt{\mathrm{diag}\left(P_{\tilde{x},k}, 1\right)} \cdot 3 \cdot \xi_{SoC} + \sqrt{diag\left(P_{\tilde{x},k}, 2\right)} \cdot \frac{dOCV^{-1}}{dSoC}\Big\vert_k \cdot 3 \cdot \xi_{V_{\mathrm{RC}}} \tag{10}$$

The multiplication by three provides a confidence interval of 99.7% (three times standard derivation $\sigma_x = \sqrt{\mathrm{Var}(x)}$). These EB may not be exact, since the noises (especially process noise) are estimated, but they change dynamically according to estimate uncertainty, and by overestimating the noises they are a conservative measure to recalibrate the SoC values from AhB. The tuning parameters $\xi_{SoC}$and $\xi_{V_{RC}}$ are included as weighting in order to adjust the EB as described earlier. The EB are smaller for high $\frac{dOCV}{dSoC}\Big\vert_k$ values, i.e. high voltage variations lead to smaller corresponding variations of

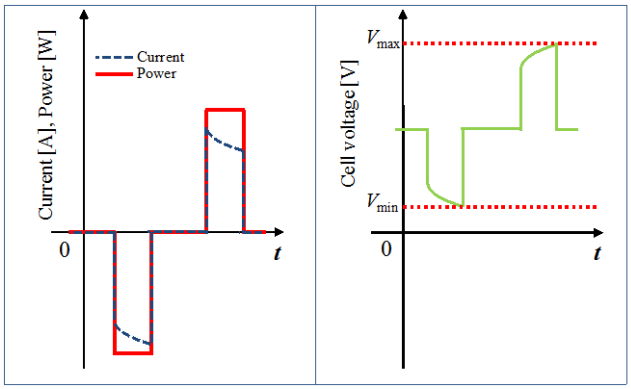

Fig. 3. Cell behaviour of a power pulse.

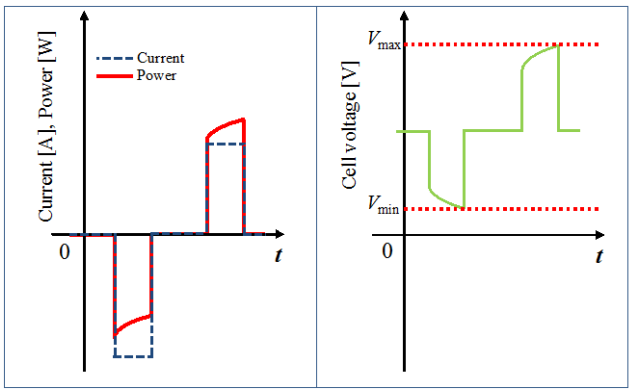

Fig. 4. Cell behaviour of a current pulse.

SoC. EB change dynamically and compensate errors caused by instability due to corrupted model parameters, since the uncertainties and the error variances will increase significantly, if the system becomes unstable. For the verification of the Kalman filter algorithm a dynamic current profile is used. In Fig. 2 the procedure of recalibration is exemplified where the AhB values are forced to be within the Kalman filter limit bounds. The correct initial SoC_{init} is 100%, but for the AhB algorithm this value was wrongly set to 80% and is represented by $SoC_{\text{AhC,alg}}$. The reference value $SoC_{\text{AhC,ref}}$ is calculated in parallel by a further Ah balancing algorithm with correct initial SoC_{init} value. After roughly 400 seconds the SoC error between $SoC_{\text{AhC,alg}}$ and $SoC_{\text{AhC,ref}}$ could be reduced to 6% from originally 20%, after 1750 seconds the error reaches a value of 1.6% (measurement error non-zero mean). Thus, a reliable SoC value can be provided as input to the power prediction algorithm in Fig. 1.

IV. State-of-Available-Power Prediction

First the definition of the overall reference scenario is presented before the new method for power prediction is introduced. It was mentioned that cell limits should be met in order to maintain the cell performance. These limits are defined by individual cell voltages, maximum charging/discharging current, temperature and SoC. Consequently, power prediction refers to the task of predicting, whether or not the safe operation area of the cell will be left, if a certain required power pulse is injected into the cell. For the electrical vehicle application the short forecasting horizon for power prediction is between a few seconds (e.g. start-stop capability for hybrids) up to half a minute (overtaking maneuver). In comparison, SoC and temperature values change with a significantly higher time constant, thus play a subordinate role in power prediction within this given time period. Therefore, state-of-available-power can be defined as the maximum power that can be applied to the battery at the current state, on condition that neither minimum/maximum individual cell voltages nor maximum rated cell charging/discharging current exceed the predefined limits. However, different possible reference scenarios (charging/discharging the cell with constant current (CC), constant voltage (CV) or a constant power (CP)) have to be considered since SoAP prediction significantly depends on future battery load behaviour and is therefore not predictable. These reference scenarios are fictitious events appearing rather seldom during battery operation in electrical vehicles. To mention only one, a CC situation would imply a infinite current change rate at the beginning of the pulse. Therefore the reference scenario for power prediction is based on constant current pulse and considered as the worst case scenario because of the following reasons:

- Current can be easily controlled and limited by the use of power electronics.
- Represents charging/discharging events with constant power, when voltage change during constant current pulse is negligible.

For that, the differences between pulses with constant power and pulses with constant current are illustrated in Fig. 3 and Fig. 4. It is shown that in order to keep the power constant, the current must be regulated during a pulse, because the cell voltage changes. Thus, for the discharging direction the current rises in amount due to the decrease of the cell voltage and for the charging direction the current behavior is exactly the opposite. As a result, the product of I_{cell} and V_{cell} is constant and the same applies to the power. In accordance with the previous considerations, the power decreases in amount during a negative current pulse, since the cell voltage drops while it increases for positive pulses. The longer a pulse lasts the higher is also the power change. In order to consider pulses with constant current and in order to grant a safety margin, the transformation of current pulses into power pulses is described as following:

$$P_{\text{pulse}} = I_{\text{pulse}} \cdot V_{\text{now}} \quad \text{for} \quad I_{\text{pulse,CHA}} > 0\,\text{A} \qquad (11)$$

$$P_{\text{pulse}} = I_{\text{pulse}} \cdot V_{\text{prog}} \quad \text{for} \quad I_{\text{pulse,DIS}} < 0\,\text{A} \qquad (12)$$

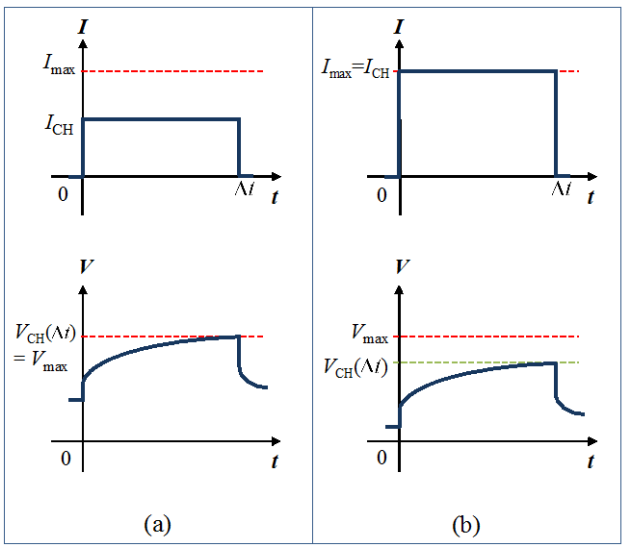

Fig. 5. (a) In case 1 the maximum operating voltage V_{max} is reached at the end of the charging current pulse with $I_{CH} < I_{max}$; (b) in case 2 the maximum operating voltage is not reached ($V_{CH} < V_{max}$) at the end of the maximum charging current with $I_{CH} = I_{max}$.

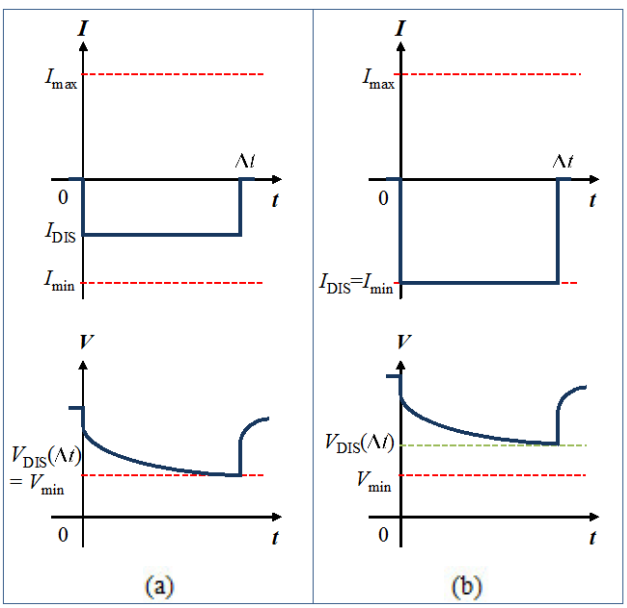

Fig. 6. (a) In *case 3* the minimum operating voltage V_{min} is reached at the end of the discharging current pulse with $I_{DIS} < I_{min}$; (b) in *case 4* the minimum operating voltage (V_{min}) is not reached for $I_{DIS} = I_{min}$.

V_{now} is the is the present cell voltage at the moment of the power prediction, which is also the lowest voltage throughout the whole pulse duration. Instead of V_{now}, "$V_{now} + I_{now} \cdot R_i$" could be chosen as well. This term leads to a smaller safety margin, but higher calculated power magnitudes. V_{prog} is the result of the voltage prognosis and it also refers to the lowest voltage during a discharging pulse. These transformation equations guarantee that a pulse with constant power P_{pulse} does not cause violation of the cell limit restrictions, presuming that the corresponding pulse with constant current I_{pulse} can be safely applied to the cell. The reason is that for P_{pulse} and for equal pulse duration, the current is in amount equal or less than I_{pulse} in any case throughout the whole pulse, and the voltage change is less in amount as well. The same considerations are applicable for the transformation of power pulses into current pulses:

$$I_{pulse} = \frac{P_{pulse}}{V_{now}} \quad \text{for} \quad I_{pulse,CHA} > 0\,A \qquad (13)$$

$$I_{pulse} = \frac{P_{pulse}}{V_{EOD}} \quad \text{for} \quad I_{pulse,DIS} < 0\,A \qquad (14)$$

The difference is that V_{prog} does not exist, since the power prediction algorithm works with current I_{pulse} as input variable. Instead of V_{prog}, the end-of-discharge voltage V_{EOD} is chosen, which is the lowest safe cell voltage.

Here, the highest possible current I_{pulse} must be identified in order to test it with the voltage prognosis algorithm. If the test is positive, P_{pulse} can be applied to the cell in any case. Hence, the denominators must refer to the smallest possible cell voltages during the pulse. The four possible cases at constant current pulse are illustrated in Fig. 5 and 6. Using equations above, the state-of-available-power prediction can be simplified to the problem of "current" prediction.

A. *Adaptive Neuro-Fuzzy Inference System*

Fuzzy inference systems (FIS) and artificial neural networks (ANN) are well-known methods for modeling

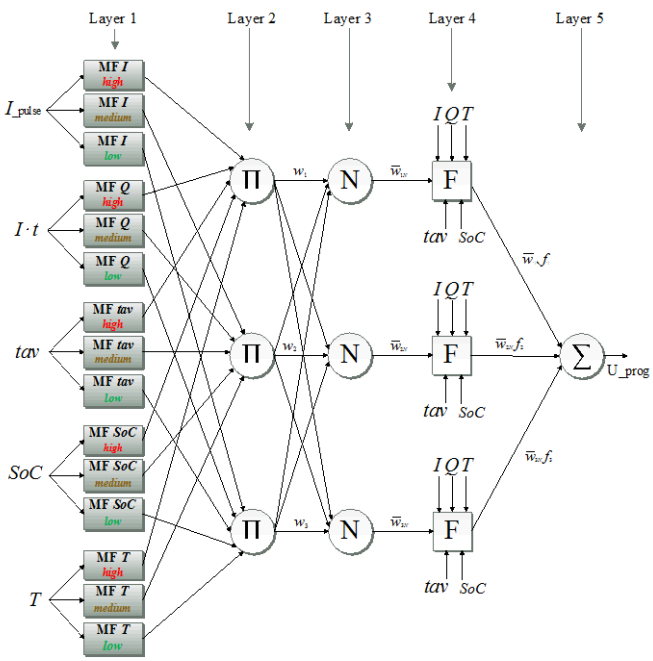

Fig. 7. Final ANFIS structure, both for negative and positive currents.

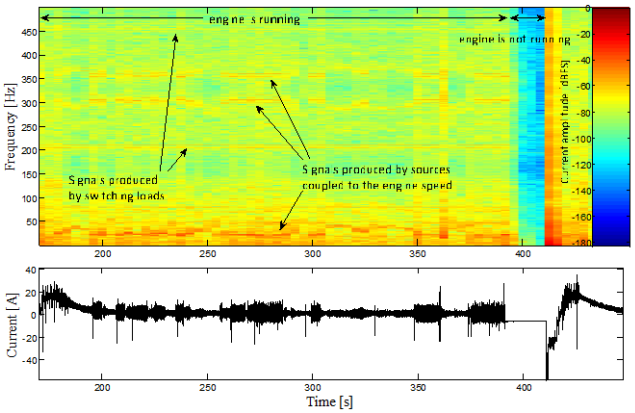

Fig. 8. Current ripple measurement across the battery of a vehicle.

non-linear systems. Fuzzy inference systems can "fuzzily" incorporate human knowledge in modeling in the kind of if-else statements, while neural networks possess the capability of learning by the use of measurement samples in order to adapt the input-output mapping to changing conditions. Combined to ANFIS, this is a highly effective tool to map input signals to output signals of a non-linear, uncertain or ill-defined system and can be used as a approximator for the battery system [13].

ANFIS Architecture: Fig. 7 illustrates the designed ANFIS with five input variables, three rules, three membership functions per input and one output for TFVP. The applied *first-order Takagi-Sugeno* type [7] of FIS, the output fuzzy sets are represented by linear functions of input variables. These function outputs are weighted using the *degrees of support* of every rule. The rule base of this ANFIS contains three IF-THEN rules, whereas each output leaving *Layer 1* correspond to one rule exemplarily expressed as:

$$\textit{Rule } 1\text{: If } \mathbf{x} \text{ is } \mathbf{A_1} \text{ and } \mathbf{y} \text{ is } \mathbf{B_1}, \text{then } \boldsymbol{f_1} = p_1 x + q_1 y + r_1$$
$$\textit{Rule } 2\text{: If } \mathbf{x} \text{ is } \mathbf{A_2} \text{ and } \mathbf{y} \text{ is } \mathbf{B_2}, \text{then } \boldsymbol{f_2} = p_2 x + q_2 y + r_2$$
$$\textit{Rule } 3\text{: If } \mathbf{x} \text{ is } \mathbf{A_3} \text{ and } \mathbf{y} \text{ is } \mathbf{B_3}, \text{then } \boldsymbol{f_3} = p_3 x + q_3 y + r_3$$

here x, y, ..., are the input variables, A_i, B_i, ..., are the fuzzy sets, $\boldsymbol{f_i}$ are the outputs within the fuzzy region specified by the fuzzy rule, p_i, q_i and r_i are the network parameters that are determined during training and adapted while battery changes its characteristics (ageing process). The parameters largely determine the mapping behavior of the ANFIS and thus must be trained in order to achieve good performance. The individual layers are designed as following [8],[9].

Layer 1: For each node *i* in this layer, three parameters need to be stored. Each parameter set defines an input membership function expressed by following equation:

$$\mu_{A_i}(x) = \frac{1}{1 + \left(\left(\frac{x - c_i}{a_i}\right)^2\right)^{b_i}} \qquad (15)$$

where x is the first input variable to the ANFIS. The membership function in equation (15) describes to which degree input x belongs to fuzzy set A_i. The parameter sets $\{a_i, b_i, c_i\}$ determine the shapes of the membership functions (here: bell-shaped).

Layer 2: Fuzzy operators are applied in order to resolve the terms in the antecedent part of each rule realized by multiplication operators. Equation (16) formulates the firing strengths as

$$\omega_i = \mu_{A_i}(x) \, X \, \mu_{B_i}(x) \, X \ldots, \quad \text{for } i = 1,2,3. \qquad (16)$$

Layer 3: The label N within each node in this layer expresses the normalized firing strength of a rule, which is calculated in the respective nodes according to equation (17):

$$\omega_{i,n} = \frac{\omega_i}{\omega_1 + \omega_2 + \omega_3}, \quad \text{for } i = 1,2,3. \qquad (17)$$

Layer 4: Here, the output of each rule is calculated based on the corresponding normalized firing strength from layer 3. The number of nodes is just equal to the number of (normalized) firing strengths, which itself is equal to the number of rules in the rule base. The node function of node *i* in this layer is expressed by following equation (implication):

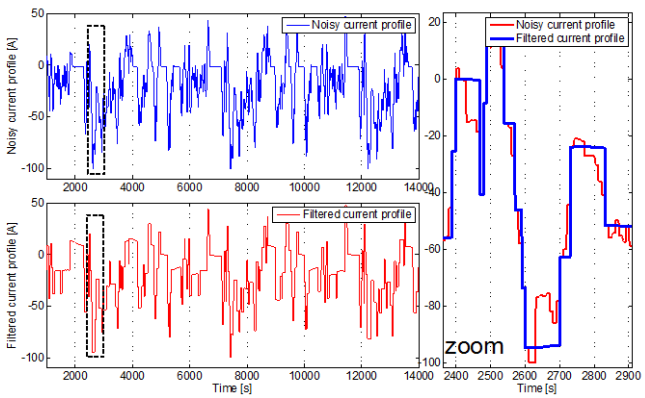

Fig. 9. Filtered current profile from noisy driving cycle using second-order low-pass filtering.

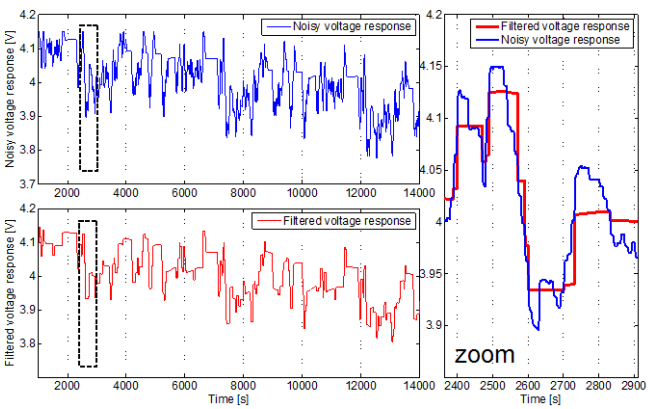

Fig. 10. Filtered voltage response from noisy driving cycle using second order low-pass filtering.

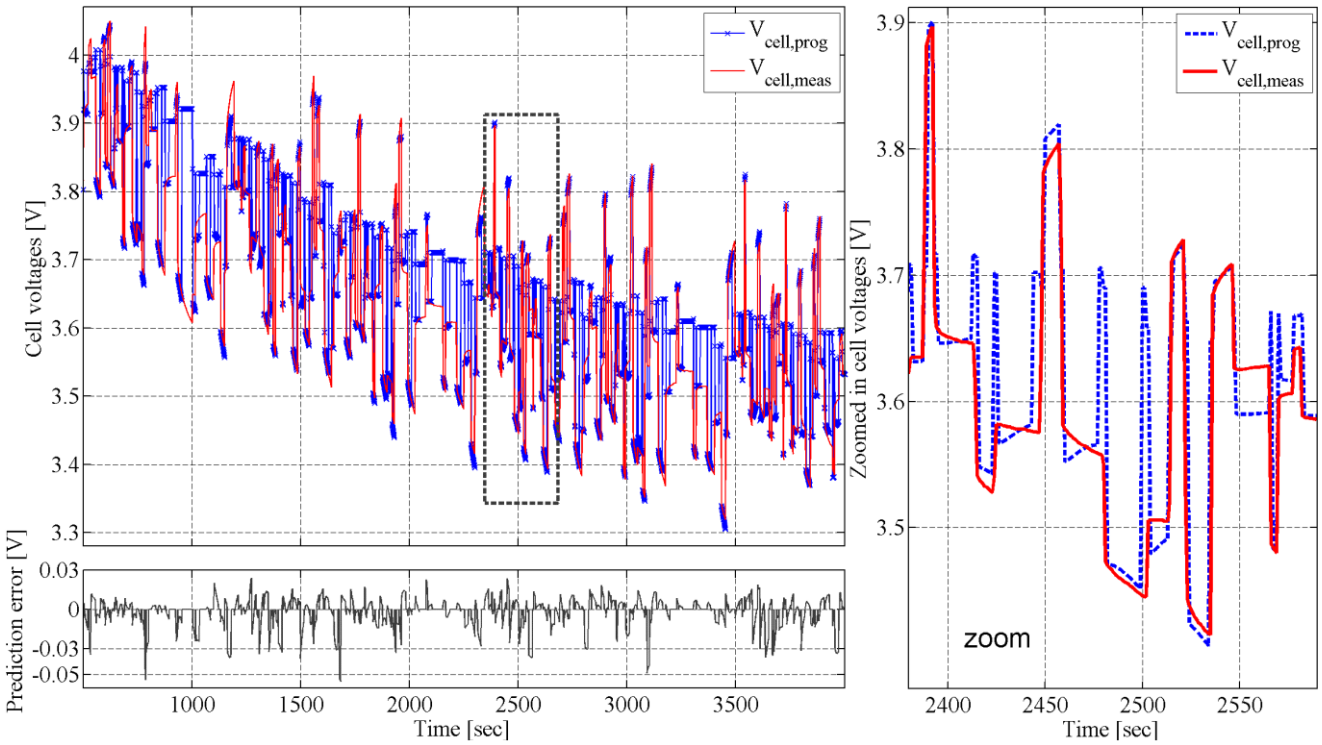

Fig. 11. On-line training results for time forward voltage prognosis (TFVP) with stop criterion Δt = 20 s, RMSE = 0:0192 V.

$$O_i^4 = \omega_{i,n} f_i = \omega_{i,n}(p_i x + q_i y + r_i) \qquad (18)$$

where O_i^4 is the is the output of rule i in layer 4. The parameter set $\{a_i, b_i, c_i\}$ describes the coefficients of a linear function of the input signals $\left(\text{here: } I_{\text{pulse}}, I \times t, tav, SoC, T\right)$

Layer 5: In layer 5 the overall output is calculated by summing up every rule output from layer 4 (aggregation).

$$O_i^5 = \sum_i \omega_{i,n} f_i = \frac{\sum_i \omega_i f_i}{\sum_i \omega_i}. \qquad (19)$$

ANFIS Learing Algorihm: A hybrid learning method is applied from [8] and further adapted according to speed and stability, which is to update the consequent parameters using the fast converging but computationally demanding least square estimate (LSE) in terms of Kalman filtering method after a forward pass of node outputs with fixed premise parameters. In the second step, the premise parameters are identified by backward passing the error rates and using gradient descent method in order to locate the minimum of the output error. Here, the modification, which is called Levenberg-Marquardt method [4],[11], is used. This method is much faster regarding convergence time.

Batch (Off-Line) Learning: In order to find an ANFIS which approximates the behavior of the system under consideration to a high degree of correctness the appropriate input signals must be identified at first. For this, the correlation analysis method well-known from the field of neural networks is used. Here, taking combinations of applicable input signals which result in the smallest root mean squared error (RMSE) after one single pass of least square estimation [10] are chosen as ANFIS input candidates. The root mean square error is calculated according to equation (20) [10]

$$\text{RMSE} = \sqrt{\frac{1}{n}\sum_{i=1}^{n} (\text{anfis}_{\text{out}} - \text{real\_data}_{out})^2} \qquad (20)$$

with n = number of training data. The final minimum RMSE value is reached for the combination of the input variables $I_{\text{pulse}}, I \times t, SoC, T$ and time averaged voltage $tav(t) = \frac{1}{t}\int_0^t V_{\text{cell}}\, d\tau$. Thus, the training data should be applied to the ANFIS consecutively epoch by epoch either until the RMSE error does not change significantly or until the cross validation

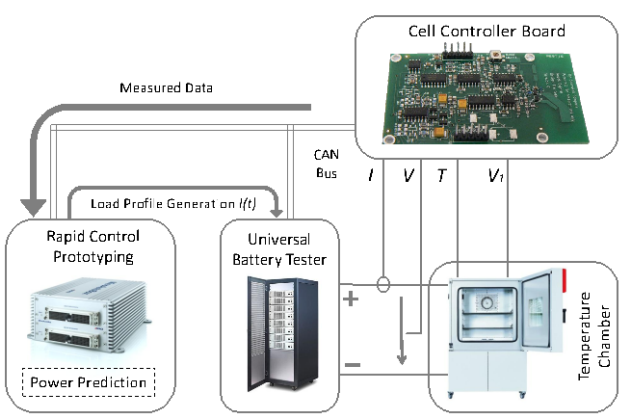

Fig. 12. Software-in-the-loop setup for SoAP verification tests.

with checking data results in RMSE increase in comparison to the previous epoch. The ANFIS structure is illustrated in Fig. 7 and the TFVP results with prognosis stop criterion of $\Delta t = 20\text{s}$ and $I_{\text{pulse}} > 10\text{ A}$ are shown in Fig. 11.

Over-fitting and Feature Grid Filtering: Over-fitting is a problem especially if the input and output data are noisy. The danger that noisy data are adapted more heavily than signal data exists. Furthermore, a problem will occur, if not the entire input space (universe of discourse) of one input variable is properly trained, but only a small region. This means, the training data might be unequally distributed. As a result, the ANFIS might be over-fitted to a certain region of the input space. As a result, the ANFIS might lose "information" of former training data. Consequently, at each time, when new training data are provided, it must be decided, if these data should be used or not. Also the training "intensity" should be varied depending on the reliability of the training data by adjusting the training parameters step size (gradient descent method), ρ (Levenberg-Marquardt) and the forgetting factor η (Kalman filter). In order to solve this problem, a feature grid filter is implemented. Basically, a two-dimensional grid map representing small ΔI areas in row direction (x-axis) and small Δt areas in column direction (y-axis). Every grid element contains information about the frequency of used training data, which matches the respective grid element. Finally, in order to determine the maximum possible power/current magnitude for a pulse of defined duration, the prediction algorithm must be run iteratively. For each new run, the magnitude of the power/current is changed towards the maximum possible value step by step using the bisection method. Signal pre-filtering for on-line data processing: In a batch learning process, which is carried out off-line, one training epoch is carried out for each combination of input candidates. The advantage of batch learning is that the training algorithm can be applied to a whole set of training data pairs at one go. Here, the ANFIS was trained with dedicated pulses and compared to desired voltage responses. However, in modern vehicles the current/voltage signals are disturbed by noise, overlaid spurious signals through switching on various loads and by the driving behaviour of the driver (uneven load through random acceleration/braking). A more detailed look at the development of the spectrum over time is shown in Fig. 8 as a spectrograma. As can be seen, there are not many distinct strong peaks at a frequency that could be used to adapt the ANFIS parameters. To provide the best possible training data, the noisy signal has to be low-pass filtered to identify strong pulse data from input signals which updates the ANFIS at each new pulse detection. The on-line filtered training signals are depicted in Fig. 9 and 10. The current profile simulates real driving conditions (acceleration, recuperation, stops) with high frequency noise. That current signal is filtered using an second-order IIR filter. The sample time is chosen to 100ms, i.e. every 100ms one training data pair is acquired (if available and required) and one output value for cell voltage prognosis is provided by the ANFIS model as long as a valid pulse is active. The requirements for a valid pulse are summarized in the following list, with time index "k" referring to the time steps following after the pulse detection, i.e. the time step, at which a new pulse is detected, is not considered:

- $I_k - I_{k-1} \leq dI_{\text{thr}}$ with $dI_{\text{thr}} = 3\text{ A}$
- $I_k \geq dI_{\text{thr}}$ with $dI_{\text{thr}} = 10\text{ A}$
- $t_{\text{min}} \leq \Delta t \leq t_{\text{max}}$ with $t_{\text{min}} = 3\text{ s}$ and $t_{\text{max}} = 20\text{ s}$
- $t_{I,\text{samp}} - t_{U,\text{samp}} < t_{\text{thr}}$, i.e. current and corresponding voltage sampling should be as close as possible; here t_{thr}=sample time.
- $T_k - T_{k-1} \leq dT_{\text{thr}}$, i.e. temperature should not change significantly during pulse.
- Operation range of battery cell not violated.

V. Real-Time Software-In-The-Loop Tests

The initial problem was to develop an adaptive algorithm, which can predict the available power under present condition. The goal of SIL tests is to verify the functionality of the proposed algorithm in real-time environment. The individual components (Fig. 12) are the cell controller board (in-house development) for gathering sensor information from battery cell (current, cell voltage and temperature), MicroAutoBox (MABX) as rapid control prototyping (RCP) hardware [15] for code testing, and battery cell under test (Kokam 53Ah Lithium Polymer SLPB120216216) placed in a temperature chamber (Binder MK 240) and connected to a universal battery tester (Digatron UBT) which performs charging and discharging in accordance to the programmed driving cycle. The overall system is interconnected via CAN-bus. A recorder function is incorporated in the MicroAutoBox, which captures and stores data during runtime. All algorithms implemented in the MABX run in real-time. The test profile shown in the top of Fig. 9 consists of 4 hr dynamic current profile followed by a rest time of 3 hr and CC/CV-charging. At first, the initial ANFIS was trained

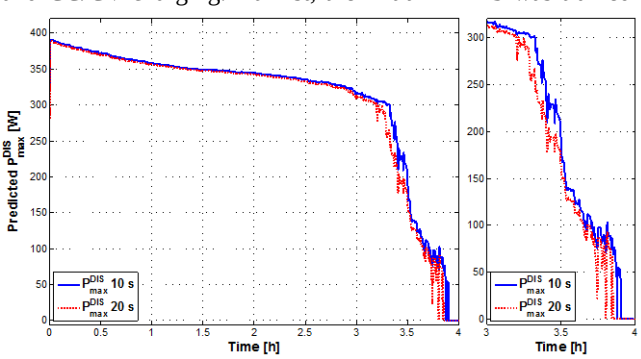

Fig. 13. Predicted maximum discharging power for driving cycle recorded by MABX.

for three epochs beforehand. Secondly, the initial error covariance matrix elements were set to higher values in order to simulate greater error oscillations. As a result, the monitoring system shows the ability to filter out the quantization noise so that an over-fitting due to noise can be avoided. The voltage prognosis algorithm proposed can test, whether certain power pulses can be injected or not, by transforming them to current pulses at first. In order to determine the maximum possible power/current magnitude for a pulse of defined duration, the prognosis algorithm must be run iteratively. For each new run, the magnitude of the power/current is changed towards the maximum possible value step by step. This technique is called bisection method. Firstly, the maximum battery certified charging/discharging current is applied and the corresponding voltage responds is predicted. Are the voltage limits violated, the maximum charging/discharging current rate is reduced, followed by a new voltage prognosis. For the discharge event, when the new prognostic voltage response does not be continued below the voltage recommended for the discharge time, a higher current rate may be applied and found in the interval $\left[\frac{I_{\max}}{2}, I_{\max}\right]$. In case the prognostic voltage response continues below the final discharging voltage, the maximum discharge current has to be found in the interval $\left[0, \frac{I_{\max}}{2}\right]$. Applying a ten-degree system for interval bisection following resolution is possible:

$$\left(\frac{1}{2}\right)^{10} \cdot 100\ \text{A} = 0.098\ \text{A} \quad (21)$$

The maximum discharging power $P_{\max}^{\text{DIS}}$ max can be calculated as following:

$$P_{\max}^{\text{DIS}}(t) = V_{\text{prog}}(\Delta t, SoC, I_{\max}, T) \cdot I_{\max}(\Delta t) \quad (22)$$

and the maximum charging power $P_{\max}^{\text{CHA}}$:

$$P_{\max}^{\text{CHA}}(t) = V_{\text{prog}}(0\ \text{s}, SoC, I_{\max}, T) \cdot I_{\max}(\Delta t) \quad (23)$$

The results in Fig. 13 show the maximum available discharging power for $\Delta t = 10$ s and $\Delta t = 20$ s. The battery gets discharged with a maximum current of 100 A (specified maximum discharging current by manufacturer: 265 A). It can be noticed that the first 2.5 hr the minimum discharging voltage is not violated and the discharging power is only limited by the battery tester. Therefore, the declining maximum discharging power ($0 - 2.5$ hr) is attributable to the fact of reduced open circuit voltage due to charge transfer.

VI. Conclusion

A novel method for power prediction of a lithium-ion cell was proposed, which is based on time forward voltage prognosis (TFVP) of the cell voltage. This approach incorporates the use of an adaptive neuro-fuzzy inference system (ANFIS). The network parameters are fully adaptable on-line to the present states of the battery (SoC, SoH, temperature). The adaptability is credited to learning algorithms from ANN theory. The capability of real-time operation of the overall system was verified on a SIL test bench showing very good results. The inaccuracy of the algorithms due to process and measurement noise are handled to a certain degree even in real-time environment using ill-defined measurement equipment. Commonly, a compromise between inaccurate measurement equipment and high algorithm performance was found.

Acknowledgment

This work has been done in the framework of the research project INGENEV funded by the Ministry of Economic Affairs, Energy, Building, Housing and Transport of the State of North Rhine-Westphalia, Germany. Responsibility for the content of this publication lies within the authors.

References

[1] W. Waag, C. Fleischer, C. Schäper, J. Berger, and D. U. Sauer, "Self-adapting on-board diagnostic algorithms for lithium-ion batteries," *Advanced Battery Development for Automotive and Utility Applications and their Electric Power Grid Integration*, Aachen/Germany, Mar. 2011.

[2] G. Ascheid and H. Meyr, "Systemtheorie I+II, 6th edition," *Druck und Verlagshaus Mainz GmbH Aachen*, Aachen/Germany, Mar. 2007.

[3] D. Simon, *Optimal State Estimation: Kalman, H Infinity, and Nonlinear Approaches*, *Wiley-Interscience*, 2006.

[4] M. T. Hagan and M. Menhaj, "Training feedforward networks with marquardt algorithm," *IEEE Trans. Neural Netw.*, Vol. 5, No. 6, pp.989-993, Nov. 1994.

[5] G. Plett, "Extended Kalman filtering for battery management systems of LiPB-based HEV battery packs: Part 1: Background," *Journal of Power Sources*, Vol. 134, No. 2, pp. 252-261, Aug. 2004.

[6] R. E. Kalman. "A new approach to linear filtering and prediction problems," *Transactions of the ASME–Journal of Basic Engineering*, Vol. 82, pp. 35-45, 1960.

[7] D. Nauck, C. Borgelt, F. Klawonn, and R. Kruse, "Neuro-fuzzy-systeme: von den grundlagen künstlicher neuronaler netze zur kopplung mit fuzzy- systemen," *Computational Intelligence, Vieweg*, 2003.

[8] J.-S. R. Jang, "Neuro-fuzzy modeling: architectures, analyses and applications," *Ph.D. Thesis*, University of California, Berkeley, 1992.

[9] J.-S. R. Jang, C.-T. Sun, and E. Mizutani, "Neuro-fuzzy and soft computing: a computational approach to learning and machine intelligence," *Prentice Hall*, 2007.

[10] J.-S. R. Jang, "Input selection for ANFIS learning," *In: Proc. Fifth IEEE Int Fuzzy Systems Conf.*, Vol. 2, pp. 1493-1499, 1996.

[11] J.-S. R. Jang and E. Mizutani, "Levenberg-marquardt method for ANFIS learning," *In: Proc. NAFIPS Fuzzy Information Processing Society*, Biennial Conference of the North American, pp. 87-91, Jun. 1996.

[12] D. U. Sauer, O. Bohlen, T. Sanders, W. Waag, R. Schmidt, and J. B. Gerschler, "Batteriezustanderkennung: mögliche verfahrens- und algorithmenansätze, grenzen der batteriezustandserkennung," *Energiemanagement und Bordnetze II, Hrsg. Matthias Schöllmann, Expert-Verlag*, pp. 1-30, 2007.

[13] J.-S. R. Jang and S. Chuen-Tsai, "Neuro-fuzzy modeling and control," *Proceedings of the IEEE*, Vol. 83, No. 3, pp. 378-406, Mar. 1995.

[14] K. Xiong, H. Zhang, and L. Liu, "Adaptive robust extended Kalman filter for nonlinear stochastic systems," *IET Control Theory Applications*, Vol. 2, No. 3, pp. 239-250, Mar. 2008.

[15] D. Abel and A. Bollig, "Rapid Control Prototyping: Methoden und Anwendungen," *Springer Verlag Heidelberg*, 2006.

[16] G. Welch and G. Bishop, "An introduction to the kalman filter," *In: Department of Computer Science, University of North Carolina*, Chapel Hill, 2006.

[17] O. Bohlen, J. B. Gerschler, D. U. Sauer, P. Birke, M. Keller, "Robust algorithms for a reliable battery diagnosis - managing batteries in hybrid electric vehicles," *22nd Electric Vehicle Symposium (EVS22)*, Yokohama, Japan, 2006.

[18] PNGV battery test manual, INEEL, *DOE/ID-10597, Rev. 3*, 2001.

[19] Advanced Technology Development Program For Lithium-Ion Batteries. Battery Technology Life Verification. *Test Manual., INEEL/EXT-04-01986*, 2005.

[20] Battery Test Manual For Plug-In Hybrid Electric Vehicles, *U.S. Department of Energy, INL/EXT-07-12536*, 2010.

[21] N. Nieto, M. Ecker, S. Käbitz, J. Münnix, and D. U. Sauer, "Detailed calendar and cycle life studies of NMC-based 18650 automotive lithium-ion batteries," *16th International Meeting on Lithium Batteries (IMLB)*, Korea, 2012.

[22] M. Broussely, Ph. Biensan, F. Bonhomme, Ph. Blanchard, S. Herreyre, K. Nechev, R. J. Staniewicz, "Main aging mechanisms in Li ion batteries," *Journal of Power Sources*, Vol. 146, No. 1-2, pp. 90-96, Aug. 2005.

[23] D. P. Abraham, J. L. Knuth, D. W. Dees, I. Bloom, and J. P. Christophersen, "Performance degradation of high-power lithium-ion cells electrochemistry of harvested electrodes," *Journal of Power Sources*, Vol. 170, No. 2, pp. 465-475, Jul. 2007.

[24] M. Safari and C. Delacourt, "Aging of a commercial Graphite/LiFePO4 cell," *Journal of The Electrochemical Society*, Vol. 158, No. 10, pp. 1123-1135, Aug. 2011.

[25] R. G. Jungst, G. Nagasubramanian, H. L. Case, B. Y. Liaw, A. Urbina, T. L. Paez, and D. H. Doughty, "Accelerated calendar and pulse life analysis of lithium-ion cells," *Journal of Power Sources*, Vol. 119-121, pp. 870-873, Jun. 2003.

[26] D. Y. Kim and D. Y. Jung, *US 7518375*, 2009.

[27] G. L. Plett, "High-performance battery-pack power estimation using a dynamic cell model," *IEEE Trans. Veh. Technol.*, Vol. 53, No. 5, pp. 1586-1593, Sep. 2004.

[28] G.L. Plett, *WO 2005050810 A1*, 2005.

[29] O. Bohlen and M. Roscher, "Method for determining and/or predicting the maximum power capacity of a battery," *US 20120215517 A1*, 2012.

[30] M. Roscher, "Verfahren zur Bestimmung und/oder Vorhersage der Hochstrombelastbarkeit einer Batterie," *DE 102009049320 A1*, 2011.

[31] R. Xiong, H. He, F. Sun, and K. Zhao, "Estimation of peak power capability of li-ion batteries in electric vehicles by a hardware-in-loop approach," *Energies*, Vol. 5, pp. 1455-1469, May 2012.

[32] F. Sun, R. Xiong, H. He, W. Li, and J. E. E. Aussems, "Model-based dynamic multi-parameter method for peak power estimation of lithiumion batteries," *Applied Energy*, Vol. 96, pp 378-386, Aug. 2012.

[33] S. Wang, M. Verbrugge, J. S. Wang, and P. Liu, "Power prediction from a battery state estimator that incorporates diffusion resistance," *Journal of Power Sources*, Vol. 214, pp. 399-406, Sep. 2012.

[34] D. Yumoto and H. Nakamura, "Estimating apparatus and method of input and output enabling powers for secondary cell," *US 7009402*, 2006.

[35] D. Yumoto and H. Nakamura, "Available input-output power estimating device for secondary battery," *US 7486079*, 2009.

[36] R. Schmidt, O. Bohlen, and D. U. Sauer, "Passive Impedanzmessung zur Batteriediagnose in Kraftfahrzeugen," *Bunsenkolloquium*, Dresden, Germany, 2007.

[37] C. Hu , B.D. Youn, J. Chung, "A multiscale framework with extended kalman filter for lithium-ion battery SOC and capacity estimation," *Applied Energy*, Vol. 92, pp. 694-704, Apr. 2012.

[38] J. Lee, O. Nam, and B. H. Cho, "Li-ion battery SOC estimation method based on the reduced order extended Kalman filtering," *Journal of Power Sources*, Vol. 174, No. 1, pp. 9-15, Nov. 2007.

[39] G. L. Plett, "Extended Kalman filtering for battery management systems of LiPB-based HEV battery packs: Part 3. State and parameter estimation," *Journal of Power Sources*, Vol. 134, No. 2, pp. 277-292, Aug. 2004.

[40] M. A. Roscher, "Zustandserkennung von LiFePO4-Batterien für Hybrid- und Elektrofahrzeuge," RWTH Aachen University, Ph.D. Thesis, 2010.

[41] M. A. Roscher, O. S. Bohlen, and D. U. Sauer, "Reliable state estimation of multicell lithium-ion battery systems," *IEEE Trans. Energy Convers.*, Vol. 26, No. 3, pp. 737-743, Sep. 2011.

[42] M. Verbrugge, "Adaptive, multi-parameter battery state estimator with optimized time-weighting factors," *Journal of Applied Electrochemistry*, Vol. 37, pp. 605-616, Feb. 2007.

[43] S. Wang, M. Verbrugge, J. S. Wang, and P. Liu, "Multi-parameter battery state estimator based on the adaptive and direct solution of the governing differential equations," *Journal of Power Sources*, Vol. 196, No. 20, pp. 8735-8741, Oct. 2011.

Christian Fleischer studied electrical and computer engineering at The Ohio State University. Since 2009 he has been working as a research associate at the Institute of Power Electronics and Electrical Drives (ISEA) in the Electrochemical Energy Conversion and Storage Systems Group. He is currently working toward his Ph.D. at RWTH Aachen University. The focus of his research is adaptive on-line state/parameter estimation for battery monitoring and management systems for lithium-ion batteries.

Wladislaw Waag studied electrical engineering at RWTH Aachen University. Since 2007 he has been working as a research associate at the Institute of Power Electronics and Electrical Drives (ISEA) in the Electrochemical Energy Conversion and Storage Systems Group. He is currently working toward his Ph.D. at RWTH Aachen University. The focus of his research is battery diagnostic and management systems for lead acid and lithium-ion batteries. Since 2008 he is a group leader and has supervised projects related to battery management systems and integration of batteries in various applications.

Ziou Bai studied electrical engineering at RWTH Aachen. He was working at the Institute of Power Electronics and Electrical Drives (ISEA) during his diploma thesis. He is currently working toward his MBA at Collège des Ingènieurs (CDI).

Dirk Uwe Sauer received his diploma in Physics in 1994 from University of Darmstadt. From 1992-2003 he has been research scientist and senior scientist at Fraunhofer Institute for Solar Energy Systems ISE in Freiburg/Germany. In 2003 he received his Ph.D. at Ulm University on battery modeling and system optimization. Since 10/2003 he is professor at RWTH Aachen University for "Electrochemical Energy Conversion and Storage Systems" at ISEA.